

A higher-order method based on local maximum entropy approximation

David González¹, Elías Cueto^{1,*}, Manuel Doblaré¹

¹ *Group of Structural Mechanics and Materials Modelling. Aragón Institute of Engineering Research (I3A). University of Zaragoza. María de Luna, 5. Campus Río Ebro. E-50018 Zaragoza, Spain.*

SUMMARY

We present here a generalization of local maximum entropy approximation for high orders of consistency (i.e., quadratic, cubic, ...). The method is based upon the application of the de Boor's algorithm to the standard, linear local maximum entropy approximation. The resulting approximation possesses some interesting properties such as non-negativity, C^∞ smoothness, exact interpolation on the boundary and variation diminishing (no Gibbs effect). The resulting structure has many similarities with B-spline surfaces, but without the tensor-product structure typical of that approximation. Examples are provided of its use in the framework of a Galerkin method showing the potential of the proposed method in solving boundary value problems. Copyright © 2007 John Wiley & Sons, Ltd.

KEY WORDS: Local maximum entropy approximation, high-order consistency, de Boor's algorithm, B-splines.

Contents

1	INTRODUCTION	2
2	LOCAL MAXIMUM ENTROPY APPROXIMATION	3
2.1	Global Maximum Entropy approximation	4
2.2	Local Maximum Entropy approximation	5
2.3	Properties of local Maximum Entropy approximations	6
2.3.1	Smoothness	6
2.3.2	Completeness	6
3	THE DE BOOR'S ALGORITHM FOR B-SPLINE SURFACES REVISITED	6

*Correspondence to: Elías Cueto. Mechanical Engineering Department. Edificio Betancourt. Universidad de Zaragoza. María de Luna, 5. E-50018 Zaragoza, Spain. e-mail: ecueto@unizar.es

Contract/grant sponsor: Spanish Ministry of Science and Innovation; contract/grant number: CICYT-DPI2008-00918

4	A MAX-ENT SCHEME WITH ARBITRARY DEGREE OF CONSISTENCY	11
4.1	Definition	11
4.2	Properties of the proposed approximation	11
4.3	The case of repeated knots	15
4.4	Approximation in non-convex domains	16
5	NUMERICAL EXAMPLES	17
5.1	Patch tests	17
5.2	Convergence tests	19
5.3	Cantilever beam	19
5.4	Approximation along non-convex boundaries: plate with a hole problem	21
6	CONCLUSIONS	24

1. INTRODUCTION

The development of approximation schemes more flexible than standard, piece-wise polynomial, finite element approximation has engaged the attention of the Computational Mechanics community during the last fifteen years [18][5][4][16]. The irruption of Moving Least Squares (MLS) approximation showed an unexpected potentiality due to its inherent flexibility (no need of a mesh in the traditional sense, smoothness of the approximation, ...) and easy construction for different levels of consistency. However, some drawbacks also appeared, such as difficulties in imposing essential boundary conditions or the development of accurate numerical integration procedures adapted for these schemes.

After more than a decade after, there still seems to be difficult to obtain a general enough approximation scheme able to verify, at the same time, desirable properties, such as positivity (verified by natural element approximations, NEM, for instance [21]), general levels of consistency (easy to obtain in Element Free Galerkin schemes, among others [5]), “exact” imposition of essential boundary conditions (again possible in NE schemes, [7] [24] [2] [1], under some weak restrictions). Note that no method among the previous verifies all the mentioned properties.

Recently, Sukumar [20] studied the use of maximum entropy (max-ent) approximation schemes in the framework of a Galerkin procedure. Max-ent schemes offer smoothness (which is not the case for NE approximations), interpolation on the boundary (which is not the case for MLS schemes, for instance) and strict positivity and variation diminishing properties (again not attainable by MLS or Reproducing Kernel Particle Methods, RKPM). However, two main limitations still hold: max-ent approximation is non-local in nature and possesses linear consistency at most. In order to avoid full matrices, Sukumar [20] proposed to use max-ent schemes over a mesh of polygons defined in the domain.

More recently, Arroyo and Ortiz [3] developed a local max-ent approximation scheme by solving the max-ent approximation in the form of a statistical inference problem in which the first order consistency is viewed as a restriction to the problem and where a parameter controlling the support of the shape function is added to the formulation. Thus, a local formulation based upon max-ent scheme is possible, but still no arbitrary degree of consistency was possible.

In their paper, Arroyo and Ortiz [3] included a fundamental theorem showing that the condition to fulfil to obtain an approximation scheme interpolating on the boundary is that the shape functions can be viewed as a convex combination, i.e., they satisfy the partition of unity property, together with the linear consistency and the non-negativity condition. This result is, in our modest opinion, of utmost importance in the development of new approximation schemes with good properties.

In parallel, we proposed recently a generalization of the Natural Element method in order to achieve a general degree of consistency [10]. This generalization is based upon the use of the de Boor's algorithm, previously used to define high-order B-spline curves by recursive use of linear interpolation. Natural neighbour shape functions are positive and satisfy the partition of unity property by construction, so the resulting scheme is a convex combination and hence the before mentioned interpolation behaviour on the boundary is obtained. In addition, B-splines are constructed as convex combinations of linear interpolants [9], so the natural neighbour interpolation proposed in [10] provides a scheme with strict interpolation on the boundary and also a general degree of consistency.

However, natural neighbour (Sibson) schemes are only C^0 , and therefore the resulting scheme is, in general, only C^0 (it is smooth everywhere, but only C^0 at the edges of the Delaunay triangles). Although a more general scheme is possible, by using the Hiyoshi-Sugihara form of natural neighbour interpolation [13], the resulting scheme is complex and of high computational cost, see [10].

Arroyo and coworkers have proposed recently a max-ent form of their interpolation scheme with second order of consistency [8], by enforcing the quadratic consistency in the statistical inference problem defining the max-ent scheme. The resulting approximation scheme conserves the interesting properties of the linear max-ent scheme (smoothness, positivity, strict interpolation on the boundary, ...) but again has no direct extension to a general degree of consistency.

Here we propose a different approach to the problem, by viewing max-ent interpolation as a suitable generalization of linear interpolation to Euclidean spaces of dimension $n \geq 2$. Thus, max-ent schemes are a valid choice for the extension of the de Boor's algorithm in order to obtain a method with all the desired properties: positivity, smoothness, general degree of consistency and, as a consequence, strict interpolation on the boundary [11]. The resulting method also bears some similarities with the structure of isogeometric finite elements [14], but avoiding the tensor-product structure typical of B-spline surfaces.

The outline of the paper is as follows: in section 2 we briefly review the standard, linear, max-ent approximation scheme. The de Boor's algorithm is then revisited in section 3, giving rise to the development of high-order max-ent schemes in section 4. Some examples of the performance of the method are shown in section 5.

2. LOCAL MAXIMUM ENTROPY APPROXIMATION

As explained in the Introduction, local max-ent schemes were derived from standard max-ent schemes, which are global in nature. Their use in the framework of Galerkin methods dates back to the original work of Sukumar [20], by constructing the interpolation over a mesh composed by polygons, over which the interpolant is built. The local max-ent interpolation is therefore reviewed first for completeness.

2.1. Global Maximum Entropy approximation

Consider a set of nodes $X = \{\mathbf{x}_1, \mathbf{x}_2, \dots, \mathbf{x}_N\} \subset \mathbb{R}^d$. Let $u : \text{conv}X \rightarrow \mathbb{R}$ be a function whose values $\{u_I; I = 1, \dots, N\}$ are known on the node set, where conv stands for the convex hull of the node set. Consider an approximation of the form

$$u^h(\mathbf{x}) = \sum_{I=1}^N \phi_I(\mathbf{x})u_I, \quad (1)$$

where the functions $\phi_I : \text{conv}X \rightarrow \mathbb{R}$ are the *shape or basis functions*. In many branches of Science and Engineering these functions are required to satisfy the zeroth and first-order consistency conditions:

$$\sum_{I=1}^N \phi_I(\mathbf{x}) = 1, \quad \forall \mathbf{x} \in \text{conv}X, \quad (2a)$$

$$\sum_{I=1}^N \phi_I(\mathbf{x})\mathbf{x}_I = \mathbf{x}, \quad \forall \mathbf{x} \in \text{conv}X. \quad (2b)$$

If these shape functions are, in addition, non-negative ($\phi_I(\mathbf{x}) \geq 0 \quad \forall \mathbf{x} \in \text{conv}X$), then, the approximation scheme given by Eq. (1) is referred to as a *convex combination*, see for instance [9].

The positivity of shape functions allows considering them as a probability measure [20]. The Shannon entropy of a discrete probability distribution is given by:

$$H(\phi) = - \sum_{I=1}^N \phi_I \ln \phi_I. \quad (3)$$

In this framework, the basis function value $\phi_I(\mathbf{x})$ is viewed as the *probability of influence of a node I at a position x* [20]. The problem of approximating a function from scattered data can thus be viewed as a problem of statistical inference. Following [3], the optimal, or least biased, convex approximation scheme (at least from the information-theoretical point of view) is the solution of the problem

$$\text{maximize } H(\phi) = - \sum_{I=1}^N \phi_I \ln \phi_I, \quad (4)$$

subject to $\phi_I \geq 0, I = 1, \dots, N,$

$$\sum_{I=1}^N \phi_I = 1,$$

$$\sum_{I=1}^N \phi_I \mathbf{x}_I = \mathbf{x}.$$

Proofs of the existence and uniqueness of the solution to this problem are given in [3].

Approximations obtained after solving the problem given by Eq. (4) are global in nature. They were used by Sukumar [20] to solve PDEs in a Galerkin framework, after tilling the domain into convex polygons. Arroyo and Ortiz [3], however, pursued a different approach, and developed a local form of the max-ent scheme by modifying the size of the support of the functions ϕ_I through the inclusion of constraints in the problem (4).

2.2. Local Maximum Entropy approximation

The locality of max-ent approximation schemes can be tuned by adding spatial correlation to the problem given by Eq. (4). In this way, the *width* of the shape function ϕ_I can be defined [3] as

$$w(\phi_I) = \int_{\Omega} \phi_I(\mathbf{x}) |\mathbf{x} - \mathbf{x}_I|^2 d\mathbf{x} \quad (5)$$

which is equivalent to the second moment of ϕ_I about \mathbf{x}_I . The most local approximation is that which minimizes

$$W(\phi) = \sum_{I=1}^N w(\phi_I) = \int_{\Omega} \sum_{I=1}^N \phi_I(\mathbf{x}) |\mathbf{x} - \mathbf{x}_I|^2 d\mathbf{x} \quad (6)$$

subject to the constraints given by Eqs. (2a), (2b) and the positivity restraint.

The new problem

$$\begin{aligned} \text{For fixed } \mathbf{x} \text{ minimize } U(\mathbf{x}, \phi) &= \sum_{I=1}^N \phi_I |\mathbf{x} - \mathbf{x}_I|^2 & (7) \\ \text{subject to } \phi_I &\geq 0, \quad I = 1, \dots, N \\ &\sum_{I=1}^N \phi_I = 1, \\ &\sum_{I=1}^N \phi_I \mathbf{x}_I = \mathbf{x} \end{aligned}$$

has solutions if and only if \mathbf{x} belongs to the convex hull of the set of points [3]. If these points are in general position, then the problem (7) has unique solution, corresponding to the piecewise affine shape functions supported by the unique Delaunay triangulation associated with the node set X (see [3] and references therein for the proof of this assertion).

The elegant solution of Arroyo and Ortiz [3] to the problem of finding a local approximation satisfying all the interesting properties of a (global) Maximum Entropy approximation is to seek a compromise between problems (4) and (7):

$$\begin{aligned} \text{For fixed } \mathbf{x} \text{ minimize } f_{\beta}(\mathbf{x}, \phi) &\equiv \beta U(\mathbf{x}, \phi) - H(\phi) & (8) \\ \text{subject to } \phi_I &\geq 0, \quad I = 1, \dots, N, \\ &\sum_{I=1}^N \phi_I = 1, \\ &\sum_{I=1}^N \phi_I \mathbf{x}_I = \mathbf{x}. \end{aligned}$$

Problems (4) and (7) are recovered by taking $\beta = 0$ and $\beta = +\infty$, respectively, as can be readily seen. Proofs of the existence and uniqueness of problem (8) are also given in the before mentioned reference.

It is important to note, however, that the evaluation of the approximation (8) does not require the solution of this problem. It is enough to solve an unconstrained minimization

problem that arises from the dual form of the problem (8). The calculation of the shape function derivatives is also explicit, see [3].

2.3. Properties of local Maximum Entropy approximations

As stated in the introduction, maximum entropy interpolation schemes solve many of the traditional problems of meshless methods. It is interesting to review here the properties of this scheme.

2.3.1. Smoothness

Proposition 2.1. *Let the parameter β to vary such that $\beta : \text{conv}X \rightarrow [0, \infty)$ be C^r in $\text{int}(\text{conv}X)$. Then, the local max-ent shape functions are of class C^r in $\text{int}(\text{conv}X)$.*

The interested reader can consult [3] for a detailed proof of this property. In addition, the max-ent shape functions recover the piece-wise linear polynomials over the Delaunay triangulation of the point set if the parameter β is set to zero. Noteworthy, the following property can be stated:

Proposition 2.2. *Let $\mathbf{x} \in \text{conv}X$. Then, $\phi_\beta(\mathbf{x})$, the minimizer of problem (8) for a parameter β , is a C^∞ function of β in $(0, \infty)$.*

The proofs of these assertions can be found in [3] and [22].

2.3.2. Completeness It is straightforward to conclude that, by construction —see Problem (8)— local max-ent approximations are linearly complete, i.e., they exactly reproduce linear polynomials. However, it is highlighted here only because this property is the basis of the consideration of max-ent approximations as a suitable generalization of linear interpolation to n -dimensional spaces. This constitutes our generalization of the de Boor's algorithm to \mathbb{R}^d .

In Fig. 1 three different max-ent shape functions are depicted. On the left, a typical shape function ϕ_I for a point located in the centre of a 7×7 regularly spaced cloud of sites. In the centre, the same for a point located on the boundary of the convex hull of the cloud. Finally, on the rightmost figure, the shape function for a site located in the corner of the cloud is depicted, showing its interpolant character for this case.

The influence of the β parameter is analyzed in Fig. 2. In it, it can be noticed that the shape functions ϕ_I take different supports. It is noticeable how, as β grows, the shape functions closely resemble the finite element shape functions, which are attained for $\beta > 4.0$ for this particular geometry of the point cloud.

3. THE DE BOOR'S ALGORITHM FOR B-SPLINE SURFACES REVISITED

It is noteworthy that local max-ent approximation schemes provide a means to control the smoothness of the approximation by tuning the support of the shape functions. Thus, if the β parameter is forced to grow, the piece-wise linear polynomials constructed over the Delaunay triangulation of the points are recovered. In the context of B-spline-like approximation, this fact will provide us with the freedom to control the smoothness of the resulting approximation. The following paragraphs revisit the basics of B-splines under the de Boor's framework.

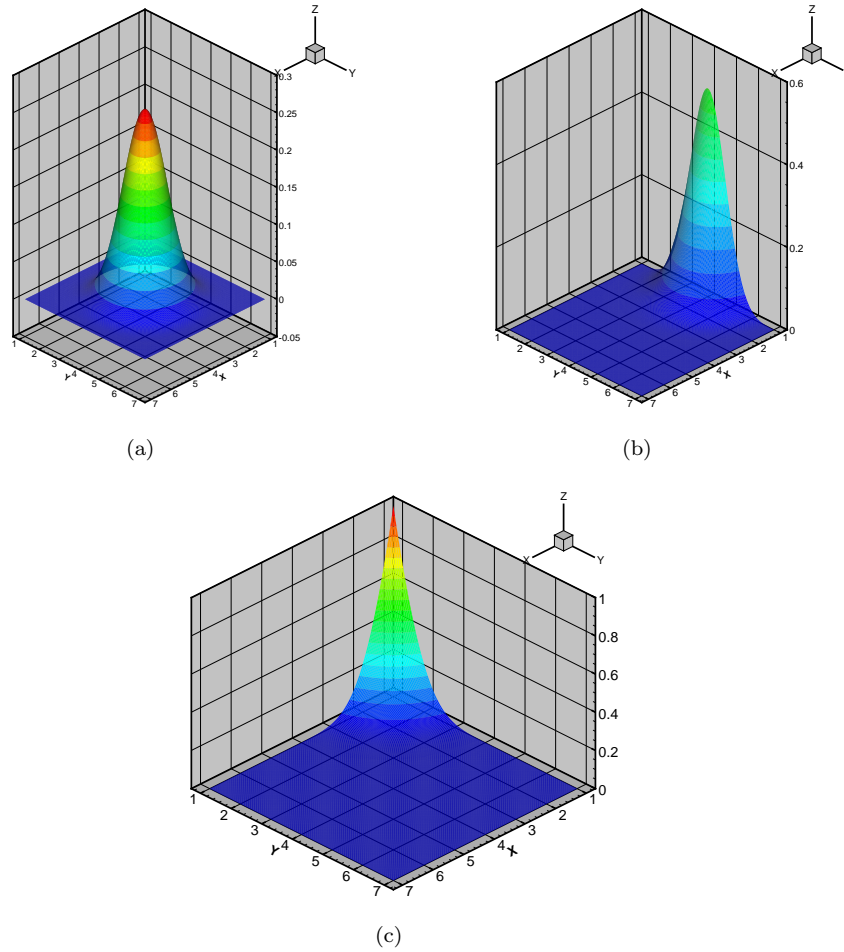


Figure 1. Shape functions on a set of 7×7 regularly distributed points. (a) Point in the centre of the cloud. (b) Point located at the boundary. (c) Node at a corner. All functions are computed for a parameter $\beta = 0.8$.

The de Boor’s algorithm constitutes a generalization of the de Castel’jau algorithm for Bézier curves, which states that such curves can be obtained by successive application of linear interpolation [9]. For a set of points $\mathbf{b}_0, \mathbf{b}_1, \dots, \mathbf{b}_n \in \mathbb{E}^3$ and $t \in \mathbb{R}$, the construction

$$\mathbf{b}_i^r(t) = (1 - t)\mathbf{b}_i^{r-1}(t) + t\mathbf{b}_{i+1}^{r-1}(t) \text{ with } \begin{cases} r = 1, \dots, n \\ i = 0, \dots, n - r \end{cases}, \quad (9)$$

where $\mathbf{b}_i^0 = \mathbf{b}_i$, gives the desired Bézier curve.

The de Boor’s algorithm introduces a parametric space, defined by an arbitrary sequence of knots (u_0, u_1, u_2, u_3 for a quadratic curve), thus generalizing this algorithm and giving considerably more freedom to the resulting set of curves. The bivariate function $\mathbf{b}[u, u]$ —

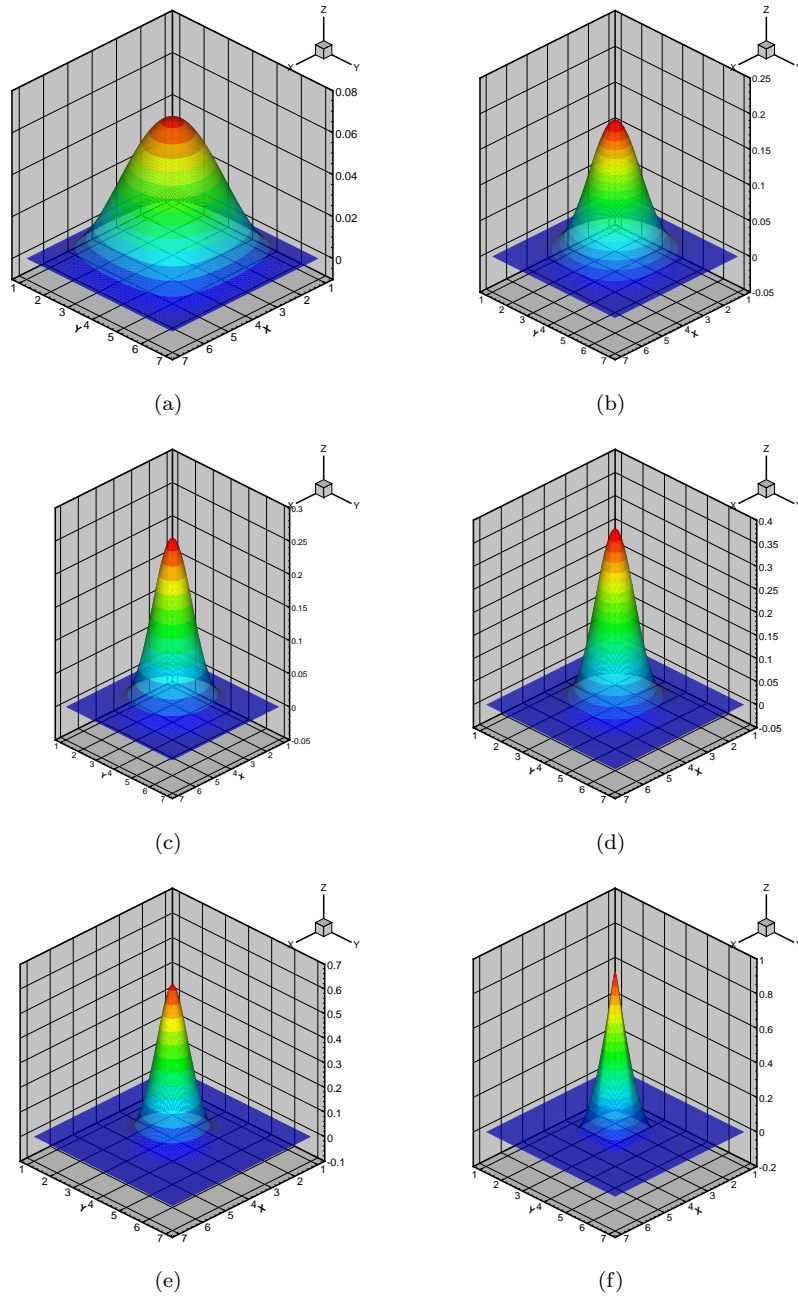


Figure 2. Influence of the β parameter on the resulting shape function. Functions $\phi_I(\mathbf{x})$ for the point located at the centre of the cloud and parameters $\beta = 0.2, 0.6, 0.8, 1.2, 2.0$ and 4.0 , respectively. Note the different supports, but also the different heights of the functions on the scale.

known as *blossom* in the CAD community— can be defined as (see Fig. 3)

$$\begin{aligned}
 \mathbf{b}[u, u] &= \frac{u_2 - u}{u_2 - u_1} \mathbf{b}[u_1, u] + \frac{u - u_1}{u_2 - u_1} \mathbf{b}[u, u_2] \\
 &= \frac{u_2 - u}{u_2 - u_1} \left(\frac{u_2 - u}{u_2 - u_0} \mathbf{b}[u_0, u_1] + \frac{u - u_0}{u_2 - u_0} \mathbf{b}[u_1, u_2] \right) \\
 &\quad + \frac{u - u_1}{u_2 - u_1} \left(\frac{u_3 - u}{u_3 - u_1} \mathbf{b}[u_1, u_2] + \frac{u - u_1}{u_3 - u_1} \mathbf{b}[u_2, u_3] \right)
 \end{aligned} \tag{10}$$

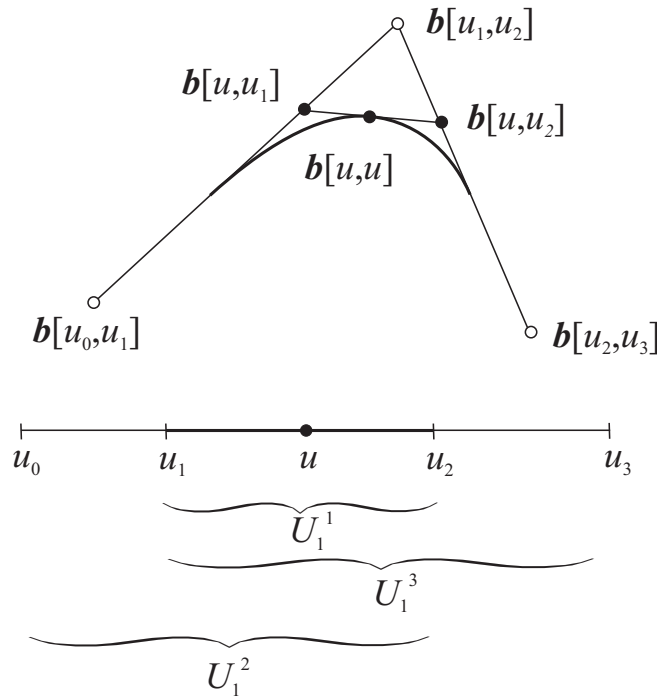


Figure 3. Schematic representation of the de Boor's algorithm.

The de Boor's algorithm expresses u in terms of intervals of growing size (three intervals, and thus four points, for a quadratic curve, four intervals for a cubic one, for instance). B-spline curves consist of a union of polynomial curve segments that join with prescribed smoothness. Following the notation in [9], let U be an interval $[u_I, u_{I+1}]$ in the sequence of knots. Then, there will be an ordered sequence of knots U_i^r , each containing u_I or u_{I+1} , such that U_i^r consists of $r + 1$ successive knots and u_I is the $(r - i)$ -th element of U_i^r .

A degree n curve segment corresponding to the interval U is then given by $n + 1$ control points \mathbf{d}_i . Each intermediate control polygon leg $\mathbf{d}_i^r, \mathbf{d}_{i+1}^r$ can then be viewed as an affine image of U_{i+1}^{n-r+1} . The point \mathbf{d}_i^{r+1} is the image of u under such an affine map.

Extending this algorithm to n -dimensional spaces ($n \geq 2$) forces us to work in non-parametric form, since the two- or three-dimensional counterpart of the intervals U are

extremely difficult to define for cases other than tensor product of one-dimensional intervals. Using the equivalence between max-ent and linear interpolation in one dimension, this simple algorithm can alternatively be obtained by applying max-ent approximation over segments U_i^r in which we eliminate $r - 1$ of the closest neighbours of the point u :

$$\begin{aligned} \mathbf{b}[u, u] &= \phi_1(u)\mathbf{b}[u_1, u] + \phi_2(u)\mathbf{b}[u, u_2] \\ &= \phi_1(u) (\varphi_0^2(u)\mathbf{b}[u_0, u_1] + \varphi_2^2(u)\mathbf{b}[u_1, u_2]) \\ &\quad + \phi_2(u) (\varphi_1^2(u)\mathbf{b}[u_1, u_2] + \varphi_3^2(u)\mathbf{b}[u_2, u_3]) \end{aligned} \quad (11)$$

where $\phi_I(u)$ represent the max-ent coordinates of point u with respect to knot I and $\varphi_I^r(u)$ represent the max-ent coordinates of point u with respect to knot I , but computed over an interval U_i^r , i.e., by eliminating $r - 1$ natural neighbours of the interval. The notation used is shown in Fig. 4.

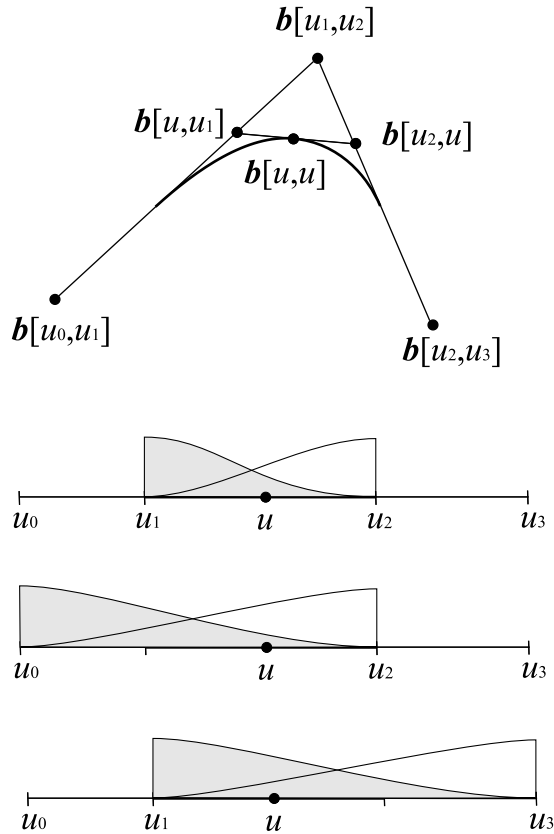


Figure 4. Schematic representation of the de Boor's algorithm employing max-ent approximation in 1D.

This algorithm will be extended to higher-dimensional cases in the following section.

4. A MAX-ENT SCHEME WITH ARBITRARY DEGREE OF CONSISTENCY

4.1. Definition

The de Boor's algorithm thus presented can be extended to higher-dimensional cases as follows. Consider again, for simplicity, a set of nodes $X = \{\mathbf{x}_1, \mathbf{x}_2, \dots, \mathbf{x}_N\} \subset \mathbb{R}^2$ and a quadratic consistency scheme (the extension to three or higher dimensions and higher-order consistency is straightforward, as will be seen). Then, we employ the same strategy as in [10] in the context of natural element methods, to construct a new family of approximation schemes, giving surfaces defined as:

$$s(\mathbf{x}) = \sum_{I=1}^n \sum_{J=1}^{n^I} N_{IJ}(\mathbf{x}) d_{IJ}, \text{ with } d_{IJ} = d_{JI} \quad (12)$$

where n represents the number of nodes contained in $\text{supp } \phi_I(\mathbf{x})$. In addition,

$$N_{IJ}(\mathbf{x}) = \phi_I(\mathbf{x}) \varphi_J^I(\mathbf{x}) \quad (13)$$

and d_{IJ} play the role of the control points in standard B-spline curves or surfaces, although their physical position is more complex to locate (except for linear and quadratic consistency, as will be demonstrated) and therefore should be considered as mere weights. Note that the true shape function will be composed by the sum of two terms, i.e., $N_{IJ}(\mathbf{x}) + N_{JI}(\mathbf{x})$. $\phi_I(\mathbf{x})$ represents the max-ent node I shape function's value at point \mathbf{x} . Functions $\varphi_J^I(\mathbf{x})$ represent the max-ent node J shape function's value at point \mathbf{x} , in the original cloud of nodes, but without the I -th node (see Fig. 5), in the sense described by the previous section. Finally, n^I is the number of nodes contained in $\text{supp } \varphi_I(\mathbf{x})$ when we eliminate the site I , similarly to the de Boor's algorithm.

Remark 1. For the cubic case, for instance, the shape functions would be $N_{IJK}(\mathbf{x}) = \phi_I(\mathbf{x}) \varphi_J^I(\mathbf{x}) \psi_K^{IJ}(\mathbf{x})$, where ψ_K^{IJ} represents the shape function associated to node K but after eliminating nodes I and J .

The typical appearance of the functions N_{IJ} described before is shown in Fig. 6 for a general set of irregularly distributed sites.

4.2. Properties of the proposed approximation

The approximation defined after Eq. (12) possesses some similarities with standard B-spline curves. These properties will be studied in this section, again with focus in the quadratic case for the sake of simplicity. In general, these properties are similar to the approximation proposed by the authors in [10], except in the degree of smoothness, but are reproduced here for completeness.

Proposition 4.1. The functions N_{IJ} form a partition of unity, i.e.,

$$\sum_{I=1}^n \sum_{J=1}^{n^I} N_{IJ}(\mathbf{x}) = 1 \quad \forall \mathbf{x} \in \mathbb{R}^2 \quad (14)$$

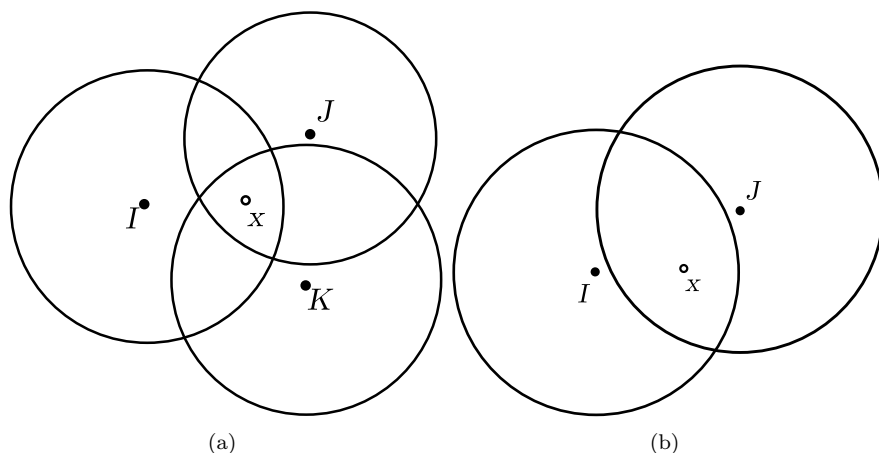


Figure 5. Schematic representation of the proposed algorithm. (a) Set of sites $\{I, \dots, N\}$. We consider an evaluation point \mathbf{x} , belonging to the support of knots I , J and K . (b) After eliminating site K , the evaluation point belongs to the support (with possibly different radius) of knots I and J only. This is an idealized case, since no point can belong to two shape function supports only in two dimensions.

Proof By applying the definition of the new basis functions, given by Eq. (13) we have

$$\sum_{I=1}^n \sum_{J=1}^{n^I} N_{IJ}(\mathbf{x}) = \sum_{I=1}^n \sum_{J=1}^{n^I} \phi_I(\mathbf{x}) \varphi_J^I(\mathbf{x}) = \sum_{I=1}^n \phi_I(\mathbf{x}) \sum_{J=1}^{n^I} \varphi_J^I(\mathbf{x}).$$

and, by using the well-known partition of unity property of max-ent approximation,

$$\sum_{J=1}^{n^I} \varphi_J^I(\mathbf{x}) = 1 \Rightarrow \sum_{I=1}^n \sum_{J=1}^{n^I} N_{IJ}(\mathbf{x}) = \sum_{I=1}^n \phi_I(\mathbf{x}) = 1. \quad (15)$$

■

This property is of utmost importance if this kind of approximation is going to be used in the approximate solution of PDEs by a standard Galerkin procedure, since it ensures that rigid-body motions are reproduced properly. Following this reasoning, we demonstrate the linear completeness of the approximation:

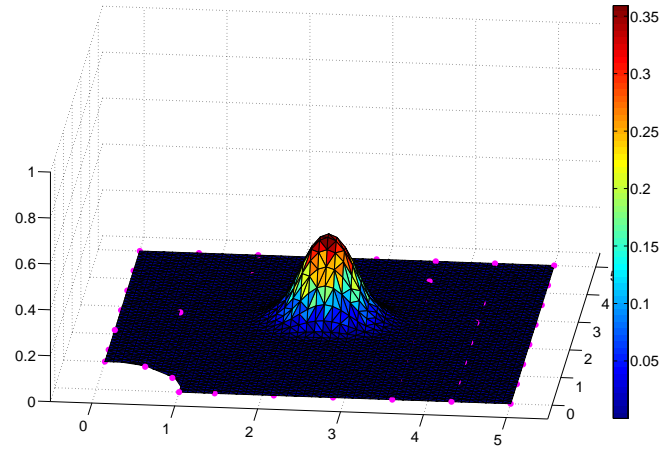
Proposition 4.2. *The basis functions $N_{IJ}(\mathbf{x})$ span the space of linear polynomials.*

Proof To prove this, we consider an approximation of the type:

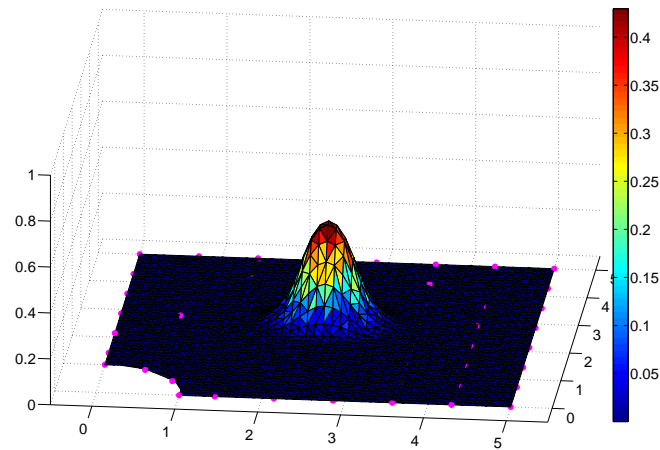
$$s(\mathbf{x}) = \sum_{I=1}^n \sum_{J=1}^{n^I} N_{IJ}(\mathbf{x}) \left(\frac{x_I^k + x_J^k}{2} \right),$$

for each coordinate x^k , where x_I^k represents the coordinate k of the node I neighboring a generic point \mathbf{x} . Thus,

$$s(\mathbf{x}) = \sum_{I=1}^n \sum_{J=1}^{n^I} \phi_I(\mathbf{x}) \varphi_J^I(\mathbf{x}) \left(\frac{x_I^k + x_J^k}{2} \right) = \frac{1}{2} \sum_{I=1}^n \sum_{J=1}^{n^I} \phi_I(\mathbf{x}) \varphi_J^I(\mathbf{x}) (x_I^k + x_J^k).$$



(a)



(b)

Figure 6. Shape of the typical functions N_{IJ} for a set of irregularly distributed sites. (a) $\beta = 4.1$. (b) $\beta = 5.2$. Note the different heights of the functions and also the different support sizes. This difference, however, is less evident than for standard, linear local max-ent shape functions.

Expanding the sums,

$$s(\mathbf{x}) = \frac{1}{2} \sum_{I=1}^n \sum_{J=1}^{n^I} \phi_I(\mathbf{x}) \varphi_J^I(\mathbf{x}) x_I^k + \frac{1}{2} \sum_{I=1}^n \sum_{J=1}^{n^I} \phi_I(\mathbf{x}) \varphi_J^I(\mathbf{x}) x_J^k.$$

Making use of the linear completeness of the max-ent approximation we arrive at

$$s(\mathbf{x}) = \frac{1}{2} \sum_{I=1}^n \phi_I(\mathbf{x}) \cdot x_I^k \cdot 1 + \frac{1}{2} \sum_{I=1}^n \phi_I(\mathbf{x}) x^k,$$

and, finally,

$$s(\mathbf{x}) = \frac{1}{2} x^k + \frac{1}{2} x^k \sum_{I=1}^n \phi_I(\mathbf{x}) = x^k. \quad \blacksquare$$

Note that in this case the “control points”, i.e., the values d_{IJ} are located at the midpoint between neighbouring nodes and have a clear physical meaning.

Following a similar approach, the quadratic completeness can be deduced and, by induction, the n -th order precision.

Proposition 4.3. *The basis functions $N_{IJ}(\mathbf{x})$ span the space of quadratic polynomials.*

Proof Let us consider now an approximation of the type:

$$s(\mathbf{x}) = \sum_{I=1}^n \sum_{J=1}^{n^I} N_{IJ}(\mathbf{x}) x_I^k x_J^l,$$

for each quadratic product $x^k x^l$ of the coordinates k, l , where x_I^k represents the k -coordinate of the node I neighboring the generic evaluation point \mathbf{x} . Thus,

$$\sum_{I=1}^n \sum_{J=1}^{n^I} N_{IJ}(\mathbf{x}) x_I^k x_J^l = \sum_{I=1}^n \phi_I(\mathbf{x}) x_I^k \sum_{J=1}^{n^I} \varphi_J^I(\mathbf{x}) x_J^l.$$

We obtain finally

$$s(\mathbf{x}) = x^k x^l,$$

thus obtaining, together with Props. 4.1 and 4.2, the desired proof for the completeness of the quadratic basis. \blacksquare

Remark 2. *Properties demonstrated so far are, essentially, the same demonstrated for higher-order natural neighbour interpolation in [10]. However, in that case, the obtained surfaces did not possess continuity higher than C^0 along the edges of the Delaunay triangulation of the sites. In this new approximation scheme, continuity is controlled by the β parameter.*

Standard B-spline curves are constructed, however, by successive application of linear interpolation. Piece-wise linear interpolation implies basis functions having C^0 continuity only. But second- and higher-order B-spline curve continuity is guaranteed by perfectly-matching piece-wise polynomial curves. Continuity can be controlled by repeated knots in the B-spline curve case. This is not the case in the proposed max-ent approximation, as mentioned before, in which the role of the β -parameter is essential in controlling the smoothness, together with the use of repeated nodes, of course.

Proposition 4.4. *The proposed surfaces, Eq. (12), possess a continuity of class C^r , of the same order of the original max-ent surfaces. If φ_J^I and ϕ_I are constructed with different degrees of continuity, r_I, r_J , then $r = \min\{r_I, r_J\}$.*

Proof Immediate, since the high-order max-ent approximation shape functions are convex combinations of standard local max-ent approximations. ■

In our computational experiments we have seen that the proposed surfaces behave very similarly to B-spline curves, i.e., the functions $N_{I,J}$ match smoothly at any point (for β sufficiently small), see Fig. 7.

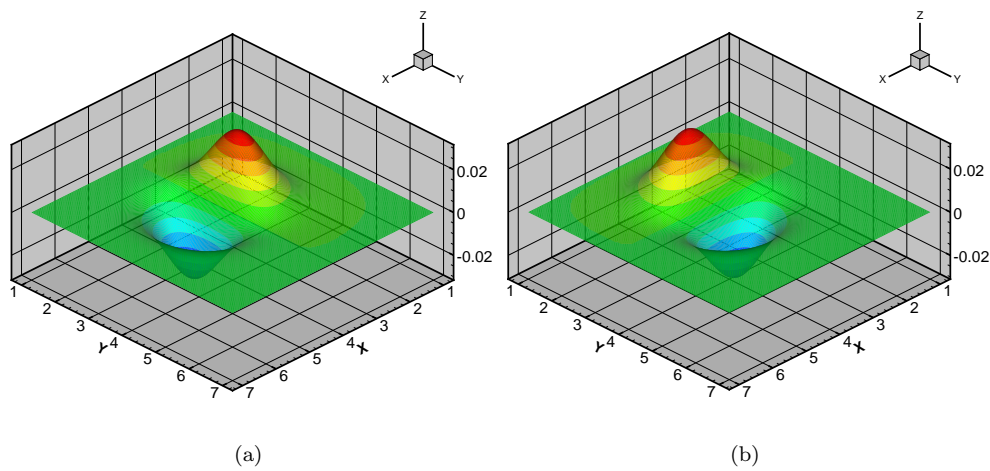


Figure 7. x and y derivatives of a typical quadratic max-ent basis function, for $\beta = 0.6$.

4.3. The case of repeated knots

It is well-known that in the case of B-splines, the continuity of the sequence of curves can be controlled by the use of repeated knots. In the proposed max-ent approximation, many new combinations arise, since the continuity for the linear case is controlled by the parameter β . If we employ C^0 linear max-ent approximation at a repeated node, an interpolating C^0 approximation is obtained.

Proposition 4.5. *If a node I is of multiplicity n and $\phi_I \in C^0$, the approximation of order n thus obtained possesses continuity C^0 and is interpolant.*

Proof Since node I is repeated, $\varphi_I^I = \phi_I$, and therefore both ϕ_I and φ_I^I belong to $C^0(\Omega)$. By construction, any convex combination of these functions will inherit the lowest continuity of both. The interpolant character follows since both functions are interpolant for the linear, C^0 case. ■

By repeating the nodes on the boundary of the convex hull of the data sites, for instance, one can make the surface to be (piecewise) quadratically interpolant along the boundary. The resulting function N_{II} for a site on the boundary is depicted in Fig. 8.

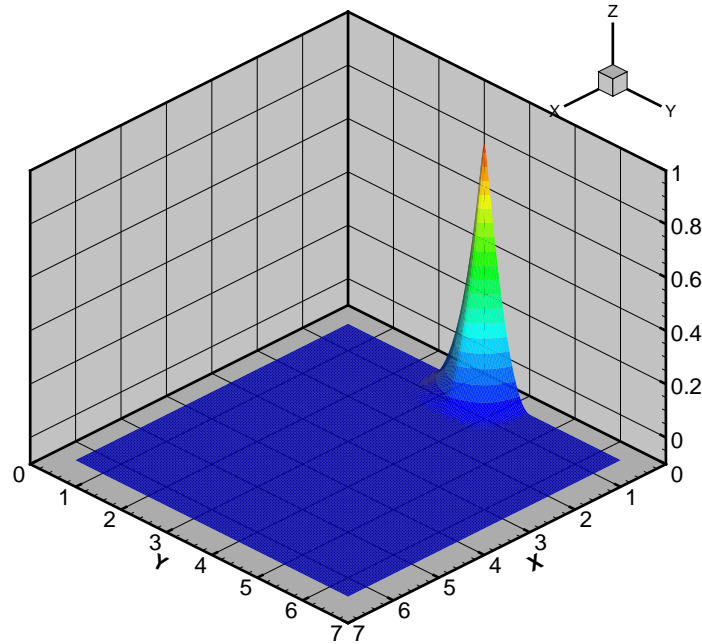


Figure 8. Interpolating quadratic function $N_{II}(\mathbf{x})$ obtained by repeating nodes on the boundary of the convex hull of the data sites. A discontinuity on the derivative appears at the node location.

This last property has again a tremendous importance when using this kind of approximation in the context of Galerkin procedures, as in the Finite Element method. The use of repeated nodes ensures interpolation and thus an easy imposition of essential boundary conditions by simply fixing the value of the approximation at the node.

Remark 3. *One property of utmost importance when dealing with B-spline surfaces is the possibility of obtaining any degree of smoothness. In the case of the proposed max-ent surfaces, this degree of smoothness can be achieved for the linear case by tuning the degree of continuity of the parameter β , as explained in Property 2.1 below. Any convex combination of C^r surfaces is C^r , so this provides a means to construct these surfaces. The issue of interpolating surfaces, however, is still controlled by repeated nodes.*

4.4. Approximation in non-convex domains

The issue of local max-ent approximation along non-convex boundaries has not been deeply studied, in our opinion. As commented before, all the definitions given for max-ent approximation are true for points on the convex hull of the nodes and nothing is said for non-convex domains. In fact, this problem arose in the very early developments of meshless

methods, and is common to the vast majority of such methods (up to our knowledge, only natural element methods are able to circumvent these problems, see [7] [24]).

In the MLS family of methods, for instance, Belytschko and coworkers proposed a method based on a visibility criterion [19], see Fig. 9, in order to seek for an appropriate measure of distance near non-convex boundaries. In essence, the idea is to avoid the neighbourhood of two nodes if it is established through a portion of the space located out of the domain. This kind of criteria produced discontinuous approximations in the context of MLS methods, although they led to a rigorous imposition of EBCs in the NEM, see [24].

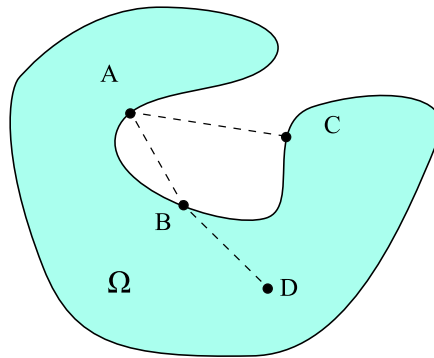


Figure 9. Visibility criterion. The boundary of the domain is considered opaque, so that nodes whose neighbourhood is established through this opaque boundary are prevented from being neighbours. Following this rule, nodes A , B and C can not become neighbours, whereas nodes B and D can.

In the case of max-ent approximations, visibility criteria produce discontinuous shape functions, just like in the MLS. A proper interpolation along non-convex boundaries is therefore still a matter of research, and is currently one of the research lines of the authors. However, for the time being, a direct solution exists. Since shape function's support are controllable through the value of the β -parameter, it can be adjusted near the boundary so as to minimize this effect, with a limit in the use of finite elements along these boundaries. The resulting shape functions for first order consistency and different β values are shown in Fig. 10.

The relative importance of the approximation along non-convex boundaries is investigated in example 5.4 in the next section.

5. NUMERICAL EXAMPLES

5.1. Patch tests

Patch tests, although originally proposed for testing the compatibility of finite element approximations [15], have been widely used in the development of meshless methods as a measure of the numerical integration error [21] [12]. It is obvious that, if a method verifies a certain given of consistency analytically, should verify exactly the patch test. If it is not the case, this must be due to the errors related to numerical integration.

Here, (displacement) patch tests have been analyzed for different nodal arrangements and for the quadratic consistency approximation, considering an elastic material given by $E = 1.0$ and

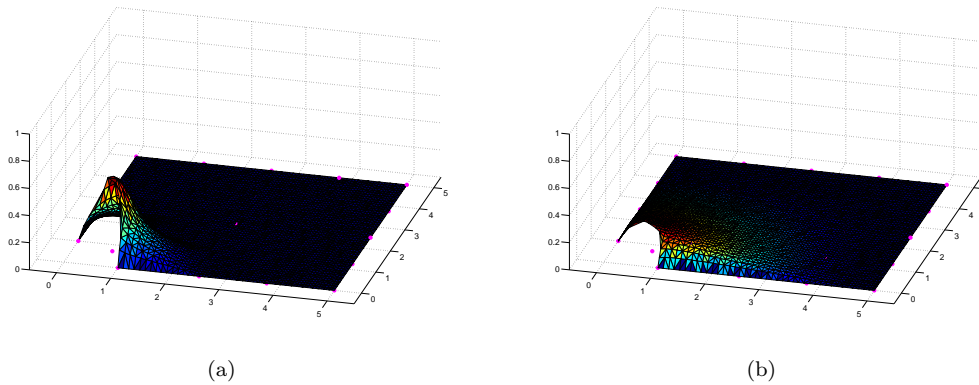


Figure 10. Resulting first-order shape function for nodes at a non-convex boundary. Low β -value (left) and high β -value (right) for the discretization of the plate with a hole problem (section 5.4).

$\nu = 0.3$. Integration has been performed by using a background grid of 20×20 cells, divided into two triangles, and three-point quadrature rules have been applied within the triangles. Results are summarized in Table I.

Cloud	$\ Error\ _{L_2}$
3×6	$3.7684 \cdot 10^{-7}$
4×4	$2.5784 \cdot 10^{-6}$
4×8	$8.1924 \cdot 10^{-6}$
5×10	$7.8942 \cdot 10^{-7}$

Table I. Results for the patch test with quadratic consistency approximants.

In analyzing these results, some considerations should be taken into account. Firstly, it is obvious that the patch tests are not passed within machine precision, as is the case with all Galerkin meshless methods and triangle-based quadratures. It is also obvious that this is due to numerical integration errors, since no other source of error exists.

Second, these errors are in good accordance with the errors reported by Arroyo and Ortiz [3] for the linear consistency approximation. No patch test result is presented by the same authors for the quadratic max-ent approximant [8]. Thirdly, these errors are computed by using a constant β -parameter. This means that increasing the number of “nodes” in the model, a much higher increase in the number of degrees of freedom is achieved (remember that the degrees of freedom can be located in the quadratic case in between the original neighbouring nodes of the cloud).

Increasing the number of integration points somewhat decreases the level of error, but not definitely. For instance, for the cloud of 5×10 nodes, a background integration mesh of 25×25 cells decreases the error up to $3.55 \cdot 10^{-5}$.

As mentioned before, the issue of numerical integration remains to be an active field of research among the meshless community, but nevertheless many meshless methods still provide very accurate results, as will be demonstrated.

5.2. Convergence tests

In order to check the convergence of the proposed approximation for problems whose solution is not spanned by the basis, we have considered the Poisson problem given by

$$-\Delta u = -6x - 6y + 2 \text{ in } \Omega = [0, 1]^2 \quad (16)$$

considering appropriate Dirichlet boundary conditions so as to have an exact solution $u = x^3 + y^3 - 2x^2 + y^2 - 2y + 1$. A dense-enough background integration mesh, composed by a grid of 420×420 squares, was employed. The squares were divided in two and three-point Hammer rules were employed.

Results for this problem are shown in Fig. 11, where a convergence rate of $R = 2.97$ for L_2 -norm has been found, in good agreement with the expected theoretical rate ($R = 3$ for L_2 -norm and quadratic approximation). For the energy norm, a slightly bigger than expected rate of convergence has been found ($R = 2.21$ in the last simulation), which is still in accordance with the theoretical values ($R = 2$).

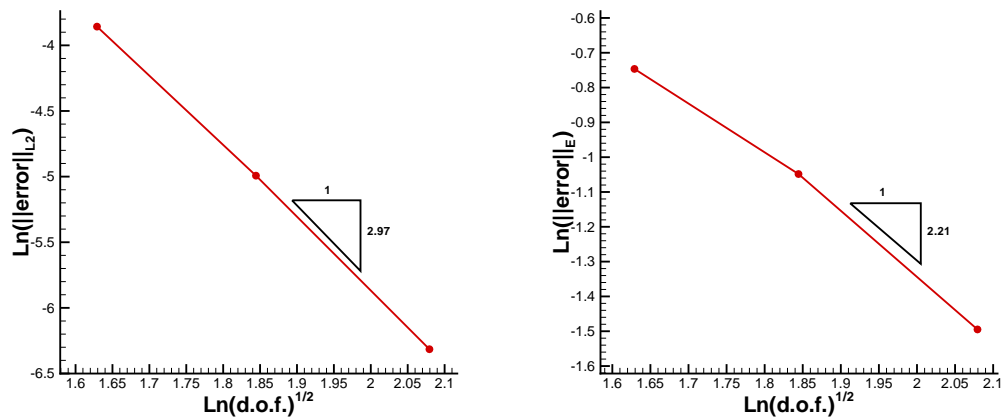


Figure 11. Convergence plot for the Poisson problem. Left, L_2 -norm of the error. Right, energy norm.

5.3. Cantilever beam

In this example we tested the behaviour of the proposed approximation against the well-known problem of a cantilever beam under bending subjected to a parabolically distributed load at one end and fixed at the other end as shown in Fig. 12.

To test the performance of the proposed formulations, we compared the results of the proposed method with quadratic consistency and the theoretical displacements at the beam

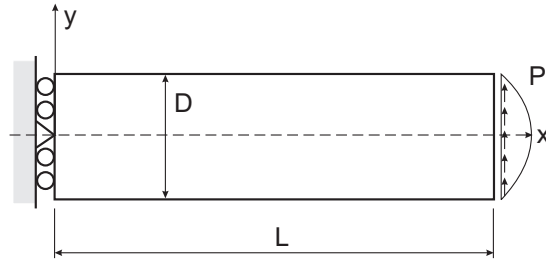


Figure 12. Geometry of the beam bending problem.

tip [23]. The analytical solution is given by:

$$\sigma_x = -\frac{Py(L-x)}{I_z} \quad (17)$$

$$\sigma_y = 0 \quad (18)$$

$$\sigma_{xy} = \frac{P}{2I_z} \left(\frac{D^2}{4} - y^2 \right) \quad (19)$$

and the displacements are given by

$$u_x(x, y) = -\frac{Py}{6E'I_z} \left[(6L - 3x)x + (2 + \nu') \left(y^2 - \frac{D^2}{4} \right) \right] \quad (20)$$

$$u_y(x, y) = \frac{P}{6E'I_z} \left[3\nu'y^2(L-x) + (4 + 5\nu') \frac{D^2x}{4} + (3L-x)x^2 \right] \quad (21)$$

where I_z represents the moment of inertia of the beam, given by $I_z = D^3/12$. For plane stress the material parameters are defined as

$$E' = \frac{E}{(1 - \nu^2)} \quad (22)$$

$$\nu' = \frac{\nu}{(1 - \nu)} \quad (23)$$

In this case, $L = 4.0$ and $D = 1.0$. Young's modulus was fixed to 1.0 and Poisson's ratio to 0.25.

For numerical integration purposes, in all the examples shown, a regular background grid of 50×50 cells was employed. Each cell was split into two triangles and standard three-point quadrature rule was employed. The objective of this technique is to avoid the numerical integration errors found in all meshless methods due to the non-polynomial character of the approximation. The use of the Delaunay triangles as integration cells was found to be clearly insufficient in order to obtain good convergence results.

The convergence results are shown in Fig. 13. Note that the convergence ratio is higher than a priori expected. This is due to the quadratic form of the solution in the vertical direction, which is reproduced analytically by the quadratic approximation employed. However, for finer discretizations, the convergence is poorer. This can be attributed to the error in the numerical integration, which is also present in this method for the numerical integration of the quadratic

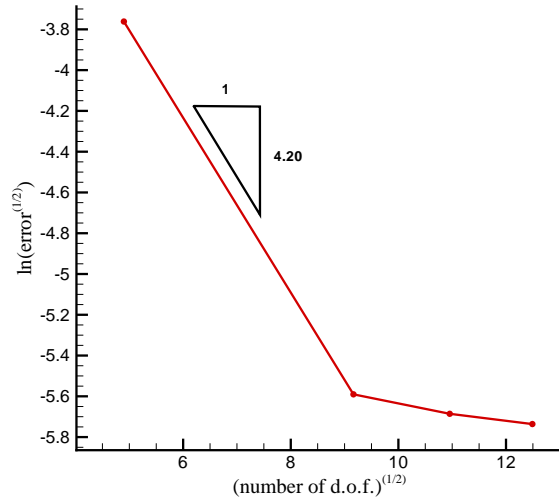


Figure 13. Convergence of the results in L_2 norm for the beam problem.

load at the beam tip. Note that this last error was not present in the case of natural elements, which in one-dimensional spaces are identical to linear finite elements, and therefore give exact quadratic polynomial approximation in one dimension. This apparent lack of convergence for finer discretizations, due to numerical integration errors is, nevertheless, not new among meshless methods, see [21] [7] [12], among other possible references. If further refinement of the integration cells is performed, results can be improved, but, as previously published in previous works [6] [17] results do not achieve the expected rate of convergence (although they are still convergent). In this case, augmenting the number of background integration cells to 80×80 , the L_2 -norm of the error decreases to -2.4934 , while augmenting to 160×160 cells gives -2.4942 .

Note also that the error levels provided by the quadratic max-ent approximation are much lower (some orders of magnitude) than the equivalent errors provided by quadratic natural elements, for instance, see [10]. This seems to confirm the Arroyo's claim for the quality of max-ent approximation and (relative) ease of integration.

5.4. Approximation along non-convex boundaries: plate with a hole problem

To clarify the issue of approximation in non-convex domains, we have studied the influence of the β parameter on the accuracy of the result for the plate with a hole problem. To this end, a cloud of 25 nodes was employed and different shape function supports—with linear and quadratic consistency—, for different β values, were tested. In all cases, a background integration mesh is used. This mesh is composed by a set of 30×30 squared cells that are, in turn, split into triangles. Three-point quadrature is used within these triangles.

The theoretical solution to this well-known problem can be found in [23], among other

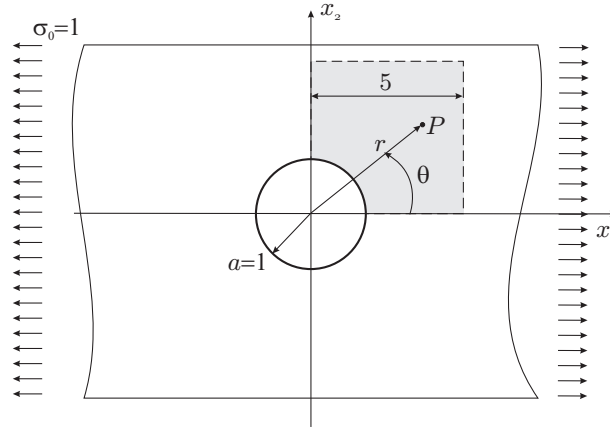


Figure 14. Geometry of the problem of an infinite plate with a hole under traction.

classical books:

$$u_1(r, \theta) = \frac{a}{8\mu} \left[\frac{r}{a}(\kappa + 1) \cos \theta + 2\frac{a}{r}((1 + \kappa) \cos \theta + \cos 3\theta) - 2\frac{a^3}{r^3} \cos 3\theta \right] \quad (24)$$

$$u_2(r, \theta) = \frac{a}{8\mu} \left[\frac{r}{a}(\kappa - 3) \sin \theta + 2\frac{a}{r}((1 - \kappa) \sin \theta + \sin 3\theta) - 2\frac{a^3}{r^3} \sin 3\theta \right] \quad (25)$$

Material parameters were Young's modulus $E=1.0$ and Poisson coefficient $\nu = 0.25$. μ represents the shear modulus and κ is the Kolosov constant, defined as

$$\kappa = 3 - 4\nu \quad (26)$$

$$\kappa = \frac{3 - \nu}{1 + \nu} \quad (27)$$

respectively, for plane strain and plane stress.

Applying symmetry conditions, only one quarter of the plate was modelled, and exact tractions were applied at the boundary of the model. The geometry of the model is shown in Fig. 14. The plate was discretized with quadratic consistency approximants and, again, repeated nodes were employed along the essential boundary.

The idea of this example relies on the fact that two nodes whose neighbourhood is established through portions of the space lying outside the domain must influence the final result, obviously decreasing the accuracy. In this way, the bigger the shape function's support is, the worst the expected accuracy.

The aim of this section is thus to clarify the true incidence of the shape function's support on the result, though different approaches are possible to elucidate this influence. In order to alleviate the influence of the β -parameter on the result, for instance, finite element-like shape functions can be used for nodes lying on the non-convex boundary —thus obtaining a true interpolation—, with the use of adaptive β values. In order to simplify the exposition as much as possible, we kept the β parameter constant over the domain and determined its influence on

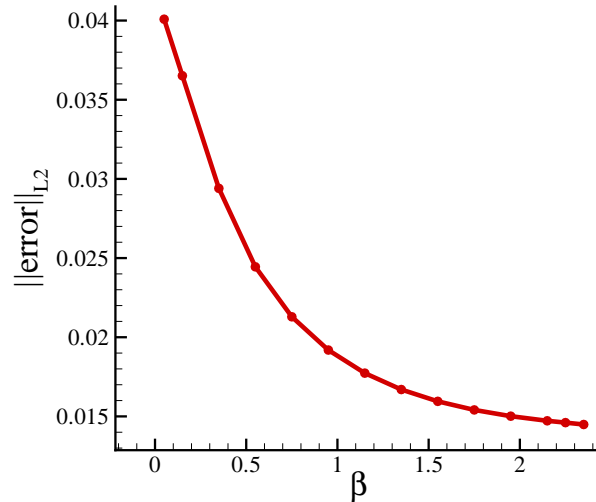


Figure 15. Convergence of the results in L_2 norm for the plate with a hole problem. Error versus β parameter for linear consistency approximation.

the final result. Of course, other sources of error can lead to misunderstanding the true sources of the final error, such as the integration error, that can vary for different shape function's support size. However, we believe that the results of this analysis allow us to have an overall impression of the influence of the size of the support when dealing with non-convex supports.

The results, for linear consistency firstly, are summarized in Fig. 15. It can be noticed that, as expected, error decreases for higher β values, and thus for smaller supports. Further refinements on the cloud size will also lead to lower errors.

A similar plot is shown in Fig. 16, but for an approximation with quadratic consistency. The error is plotted in L_2 -norm and in the discrete 2-norm (mean of the squared root of squared nodal errors), to eliminate the error associated with the integration of the error itself. In this case the effect of the β -parameter is not so clear, and there seems to be an optimum value from the point of view of accuracy. This minimum is interpreted, according to our experience, as related to the influence of the linear shape function's support on the resulting support of the quadratic shape functions, and therefore on the quadrature error. Smaller supports seem to minimize the issues related to non-convex geometry, but in turn increase the presence of small quadratic shape function's supports and therefore the quadrature error, thus generating an optimum in between.

This example provides an overall impression of the influence of the support on the accuracy of the proposed method. Since no method is currently available, up to the authors' knowledge, to exactly integrate this kind of non-polynomial approximations, there is no way to determine the relative influence of the integration error on the result.

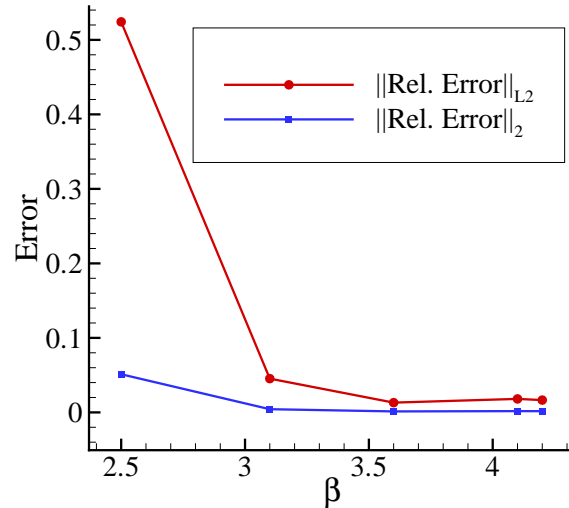


Figure 16. Convergence of the results in L_2 norm for the plate with a hole problem. Error versus β parameter for quadratic consistency approximation.

6. CONCLUSIONS

In this paper we analyze a new method of generating local maximum-entropy-based approximations with high order of consistency based on the de Boor's algorithm. The method is general and can lead to any degree of consistency. Smoothness is also controllable by means of the use of, on one hand, the β -parameter typical of max-ent approximations and, on the other, the use of repeated nodes, as in a B-spline framework. Thus, a new type of meshless approximation, strictly positive and interpolant along the boundary, is developed. This constitutes, to the best of our knowledge, the only meshless method verifying these properties (with the only exception of Arroyo and Ortiz's quadratic max-ent approximation [8], that has no further generalization to higher-order consistency).

We have presented several examples of the performance of the new approximation. In particular, we have focused in analyzing the error related to numerical quadrature of the weak form of the problem and also the method's behaviour along non-convex domains, an issue not properly studied so far. It has been noticed that the approximation along non-convex domains is affected by the size of the shape function's support, although this error is partially obscured by the quadrature error typical of meshless methods and has not been definitely quantified.

In any case, the proposed max-ent Galerkin schemes seem to constitute an appealing choice in the family of meshless methods. They combine the low computational cost with the generality of the approximation, in terms of both consistency and smoothness, and also the ease in the imposition of essential boundary conditions. The issue of numerical integration, which is nevertheless common to all Galerkin meshless methods, remains to be an issue that

deserve further efforts of research.

REFERENCES

1. I. Alfaro, D. Bel, E. Cueto, M. Doblaré, and F. Chinesta. Three-dimensional simulation of aluminium extrusion by the alpha-shape based natural element method. *Computer Methods in Applied Mechanics and Engineering*, 195(33-36):4269–4286, 2006.
2. I. Alfaro, J. Yvonnet, F. Chinesta, and E. Cueto. A study on the performance of natural neighbour-based Galerkin methods. *International Journal for Numerical Methods in Engineering*, 71(12):1436–1465, 2007.
3. M. Arroyo and M. Ortiz. Local maximum-entropy approximation schemes: a seamless bridge between finite elements and meshfree methods. *International Journal for Numerical Methods in Engineering*, 65:2167–2202, 2006.
4. T. Belytschko, Y. Krongauz, D. Organ, M. Fleming, and P. Krysl. Meshless methods: An overview and recent developments. *Computer Methods in Applied Mechanics and Engineering*, 139:3–47, 1998.
5. T. Belytschko, Y. Y. Lu, and L. Gu. Element-Free Galerkin Methods. *International Journal for Numerical Methods in Engineering*, 37:229–256, 1994.
6. Jiun-Shyan Chen, Cheng-Tang Wu, Sangpil Yoon, and Yang You. A stabilized conforming nodal integration for galerkin mesh-free methods. *International Journal for Numerical Methods in Engineering*, 50:435–466, 2001.
7. E. Cueto, M. Doblaré, and L. Gracia. Imposing essential boundary conditions in the Natural Element Method by means of density-scaled α -shapes. *International Journal for Numerical Methods in Engineering*, 49-4:519–546, 2000.
8. C. J. Cyron, M. Arroyo, and M. Ortiz. Smooth, second order, non negative meshfree approximants selected by maximum entropy. *International Journal for Numerical Methods in Engineering*, accepted for publication, 2009.
9. G. Farin. *Curves and surfaces for CAGD*. Morgan Kaufmann, 2002.
10. D. González, E. Cueto, and M. Doblaré. Higher-order Natural Element Methods: towards an isogeometric meshless method. *International Journal for Numerical Methods in Engineering*, 74(13):1928–1954, 2008.
11. D. González, E. Cueto, and M. Doblaré. Maximum entropy-based B-spline surfaces. *Computer Aided Geometric Design*, submitted, 2008.
12. D. González, E. Cueto, M. A. Martínez, and M. Doblaré. Numerical integration in Natural Neighbour Galerkin methods. *International Journal for Numerical Methods in Engineering*, 60(12):2077–2104, 2004.
13. H. Hiyoshi and K. Sugihara. Two generalizations of an interpolant based on Voronoi diagrams. *International Journal of Shape Modeling*, 5(2):219–231, 1999.
14. T. J. R. Hughes, J. A. Cottrell, and Y. Bazilevs. Isogeometric analysis: CAD, finite elements, NURBS, exact geometry and mesh refinement. *Computer Methods in Applied Mechanics and Engineering*, 194:4135–4195, 2005.
15. B. Irons and A. Razzaque. Experience with the patch test for convergence of finite elements. In A. K. Aziz, editor, *The mathematical Foundations of the Finite Element Method with Applications to Partial Differential Equations*, New York, 1972. Academic Press.
16. W. K. Liu and Y. Chen. Wavelet and multiple scale reproducing kernel methods. *International Journal for Numerical Methods in Fluids*, 21:901–931, 1995.
17. M. A. Martínez, E. Cueto, I. Alfaro, M. Doblare, and F. Chinesta. Updated Lagrangian free surface flow simulations with Natural Neighbour Galerkin methods. *International Journal for Numerical Methods in Engineering*, 60(13):2105–2129, 2004.
18. B. Nayroles, G. Touzot, and P. Villon. Generalizing the finite element method: Diffuse approximation and diffuse elements. *Computational Mechanics*, 10:307–318, 1992.
19. D. Organ, M. Fleming, T. Terry, and T. Belytschko. Continuous meshless approximations for nonconvex bodies by diffraction and transparency. *Computational Mechanics*, 18:1–11, 1996.
20. N. Sukumar. Construction of polygonal interpolants: a maximum entropy approach. *International Journal for Numerical Methods in Engineering*, 61(12):2159–2181, 2004.
21. N. Sukumar, B. Moran, and T. Belytschko. The Natural Element Method in Solid Mechanics. *International Journal for Numerical Methods in Engineering*, 43(5):839–887, 1998.
22. N. Sukumar and J. B. Wets. Deriving the continuity of maximum-entropy basis functions via variational analysis. *SIAM Journal of Optimization*, 18(3):914–925, 2007.
23. S. Timoshenko and J. N. Goodier. *Teoría de la Elasticidad*. Editorial Urmo, Spain, 1972.
24. J. Yvonnet, D. Ryckelynck, P. Lorong, and F. Chinesta. A new extension of the Natural Element method for non-convex and discontinuous problems: the Constrained Natural Element method. *International Journal for Numerical Methods in Engineering*, 60(8):1452–1474, 2004.